EXAFS investigation of the thermally induced structuring of titanium doped amorphous carbon films

C. Adelhelm[a,*], M. Balden[a], M. Sikora[b,c]

[a]*Max-Planck-Institut für Plasmaphysik, EURATOM Association, Boltzmannstr. 2, D-85748 Garching, Germany*

[b]*European Synchrotron Radiation Facility, 6 rue Jules Horowitz, 38043 Grenoble, France*

[c]*AGH University of Science and Technology, Av. Mickiewicza 30, 30-059 Krakow, Poland*

Abstract

Amorphous carbon layers doped with 8.5 at% titanium (a-C:Ti) were produced by dual-source magnetron sputter deposition. To investigate the local atomic environment of Ti, EXAFS analysis was performed for as-deposited layers and after annealing to 700, 1100 and 1300 K, as well as for Ti and TiC bulk samples. After deposition of the a-C:Ti films, most Ti atoms are homogeneously distributed in an amorphous carbon matrix. Annealing to 700 K slightly increases the order in the Ti environment, but TiC-like crystallization is hardly existent. After annealing to 1100 K, clear correspondence to the TiC standard is observed. Annealing to 1300 K further increases the order and TiC crystallite size. Fitting of EXAFS data to a theoretical model was used to derive quantitative parameters for a-C:Ti layers, e.g. Ti-C and Ti-Ti distances and ordering parameters.

1. Introduction

Nanostructured metal-doped amorphous carbon films are of great interest in different application fields. They show excellent tribological properties [1], [2], [3], exhibit increased electrical conductivity [4], and are promising systems for electrocatalytic sensors [5].

Our special interest in such films is motivated by research on the chemical erosion process of carbon by hydrogen impact. This is of great importance for future fusion devices like ITER, where carbon is part of the plasma-facing interior [6]. The reaction of hydrogen species with carbon from the first wall leads to its degradation and to formation of undesired hydrocarbon layers, depositing in the reactor vessel. If radioactive tritium is used – the fuel for fusion – this is of high safety relevance. Doping of graphite with carbide-forming transition metals is a possibility to decrease its reactivity against hydrogen species [7], [8]. To elucidate the underlying mechanism, erosion experiments were performed with hydrogen-free, metal-doped amorphous carbon layers (a-C:Me), produced by dual-source magnetron sputter deposition [9]. Their reactivity against hydrogen is determined by the kind of metal and its concentration, but also the nanoscopic structure of these layers should have influence. Therefore, their characterization down to atomic scale is required. Because erosion experiments are performed at elevated temperatures, our emphasis lies on the structural changes induced by thermal treatment.

Earlier investigations by Stüber et al. [10] deal with microstructure and properties of low friction TiC-C coatings with Ti concentrations ≥ 23 %. Recently, Feng and coworkers [11] reported about structural investigations on a-C:Ti layers with varying Ti

concentration down to 1 %. Similar studies were performed with hydrogen containing films [12].

In this paper we report about investigations on the thermal induced structuring of a-C:Ti films using X-ray absorption fine structure spectroscopy (EXAFS) and X-ray diffraction (XRD).

2. Experimental

Ti-doped amorphous carbon layers were produced by dual source magnetron sputter deposition using a Ti and a graphite target. A detailed description of the experimental setup and general deposition procedure can be found in [13]. Layers were deposited at floating potential on polished pyrolytic graphite and Si (100) wafers, ultrasonically cleaned for 3 minutes in isopropanol before deposition. To avoid influences of the substrate and surface effects during annealing (e.g. Ti oxidation), sandwich-like triple-layers with a 8.5 at% Ti doped amorphous carbon layer (a-C:Ti) between two pure amorphous carbon layers (a-C) were deposited: 210 nm a-C / 325 nm a-C:Ti / 340 nm a-C / substrate. The sandwich layer is produced by switching on and off the metal sputter source, while C is continuously deposited. Before deposition, substrate and cathode materials were cleaned by Ar^+ plasma etching. Base pressure in the chamber was $2x10^{-5}$ Pa before deposition and 0.1 Pa during the deposition process. The maximum temperature during deposition of the interlayer was 320 K. The protecting pure a-C layer on top of the a-C:Ti layer of interest does not cumber analysis by XRD, RBS and EXAFS.

The samples were annealed under vacuum (10^{-5} Pa) at 700, 1100 and 1300 K for 2 hours after deposition.

Layer composition, thickness, and homogeneity were determined by Rutherford Backscattering Spectroscopy (RBS) with 4 MeV He^+ and a backscattering angle of 165 °. Data modeling to derive layer thickness and atom concentration was performed using the program SIMNRA [14].

The crystallographic phase was investigated by XRD. Phase determination was done by comparison with the JCPDS ICDD database. The crystallite size was received by using Scherrer's formula [15] under the assumption that the width of the XRD peak is determined by the crystallite size.

EXAFS measurements on the titanium *K*-edge were performed with doped layers, Ti foil and TiC on E4 beamline at HASYLAB, DESY, Hamburg. The spectra were recorded between 4800 and 5800 eV using Ti $K\alpha_{1,2}$ fluorescence yield. The software ATHENA [16] was used for spectra normalization and background correction (AUTOBK algorithm). Fitting of EXAFS data to a calculated TiC model was performed with ARTHEMIS [16]. The spectra of pure TiC and Ti were corrected for self-absorption using the Fluo algorithm implemented in ATHENA. FEFF 8.2 [17] was used to calculate the theoretical scattering paths of a TiC cluster of 80 atoms. The FEFF input file was created using ATOMS [18] and TiC crystallographic data (database ICSD No. 1546).

3. Results and discussion

The morphology of the samples has been studied using SEM (Fig. 1). Columnar structure of the whole layer is clearly visible, no influence of the Ti-doped interlayer on layer growth is observed. On silicon substrates the surface is much smoother due to the very low roughness of the silicon wafer.

RBS analysis of the as-deposited layer reveals the composition of the interlayer: Ti 8.5 at%, Ar 0.5 at%, O 1 at%, other metals < 0.15 at%. Ti is homogeneously distributed in the doped interlayer. Measurements at different positions revels perfect lateral uniformity. Annealing leads to degassing of Ar which is introduced during deposition. No increase in oxygen concentration was observed in the heated samples. If we assume that all oxygen is bonded as TiO_2 to titanium, less than 6 % of all Ti atoms have oxygen atoms as a first neighbor, which is important for EXAFS analysis. In the annealed layers no significant Ti diffusion occurred from the Ti-containing layer into the pure carbon layers (< 20 nm).

Fig. 2 shows XRD spectra of a-C:Ti layers annealed at 1100 K and 1300 K. The positions of the three most intense TiC peaks (PDF # 321383) are added for comparison. The graphite substrate leads to peaks at 48°, 53° and below 30°. Only for the highest annealing temperature distinct carbide peaks appear in the spectrum, but only with low intensity and broad peak width. The crystallite size for the 1300 K annealed sample is estimated to ~ 3.5 nm.

Fig. 3 shows Ti *K*-edge XAS spectra of different a-C:Ti layers in as-deposited state and after annealing to 700, 1100 and 1300 K. Spectra of pure Ti and TiC were added for comparison. All spectra were normalized to unit edge jump. For the as-deposited sample almost no oscillations after the edge is observed, except a broad feature located at 5035 eV. This corresponds to a strong amorphous environment of the Ti atoms. After heating to 700 K an additional peak occurs at 5000 eV, which is probably as well present in the broad shoulder after the edge in the as-deposited sample. For layers annealed to 1100 and 1300 K the strong oscillations show clear correspondence to those

of pure TiC. The difference of both to TiC is mainly in oscillation intensity, which is increasing with annealing temperature.

The near-edge region (XANES) and, therefore, the position of the absorption edge is sensitive to the electronic structure of the absorber atom (chemical shift). Comparison of the edge position gives a qualitative representation of the electron density localized at the Ti atom. For all spectra shown in Fig. 3, the edge energy E_0 was determined by setting it to the value of the half edge jump intensity. This procedure is somehow arbitrary, there exist different methods of defining E_0 [16]. Also self-absorption correction influences its determination and the received E_0 represents an average of all Ti atoms, with possibly different electronic states. Therefore, comparison can only be done in a qualitative way. Fig. 4 shows E_0 values for all a-C:Ti specimen and for Ti and TiC. A clear trend of increased E_0 for higher annealing temperatures is visible. This corresponds to stronger Ti-C interaction, i.e. decreased electron density on Ti, which is in line with stronger TiC like bonding environment for higher annealing temperatures.

In Fig. 5 the k^2-weighted EXAFS ($k^2\chi$) as a function of photoelectron wave number k is shown for all specimens. Also the FEFF calculated EXAFS of TiC, TiC_{calc}, is included. $k^2\chi$ was derived by subtracting a background function using the FEFF calculated TiC as standard.

The situation is similar as for the normalized absorption spectra in Fig. 3: The as-deposited sample exhibits only two weak and broad maxima, which should be mainly due to the oscillation resulting from the first backscatterer, e.g. C. After annealing to 700 K additional features occur, but only with low amplitude. For the 1100 K sample all oscillations as for the TiC standard are present, differences are primarily reduced oscillation intensity. Heating to 1300 K leads to a further increase in oscillation

intensity. Deviations from TiC standard are stronger for higher k because components at higher k come from larger Ti – scatterer distances. The TiC_{calc} EXAFS represents very well the measured one. Differences (e.g. feature at 5.8 $Å^{-1}$) results from the restricted size of the calculated TiC cluster (80 atoms, 6 Å), which is of course smaller than the average grain size in the TiC bulk sample and also smaller than crystallite sizes in 1100 and 1300 K annealed samples.

In Fig. 6 the magnitude of the Fourier transform of $k^2\chi(k)$ is shown for k= 3 – 10 $Å^{-1}$ using a Hanning window for FT. In this graph data for all specimen and TiC_{calc} are represented as a function of radial distance R from Ti in real space. Because data is not corrected for phase shift, this results in graphs shifted for ~ 0.4 Å to lower R [19]. Starting with the TiC spectrum, the peaks at ~ 1.7 and 2.5 Å are attributed to the first two coordination shells of Ti which means 6 C atoms as first and 12 Ti atoms as second neighbor. For bulk Ti, the carbon signal is of course missing. TiC_{calc} represents very well the measured one up to 5 Å, which is the size of the calculated cluster. For the a-C:Ti layers there is again spectral correspondence to the TiC standard: Up to ~8 Å for 1300 K and up to ~7 Å for 1100 K annealing temperature. For the 700 K annealed layer, the signal of the first Ti neighbor is present, but broader and with smaller intensity. The spectrum of the as-deposited sample shows a further decreased intensity of the Ti peak and a significant smaller Ti-Ti distance.

To derive more quantitative information, fitting of the first two coordination shells (Ti-C and Ti-Ti) of TiC_{calc} to experimental data was performed. Because the self-absorption correction, applied for the TiC standard sample, strongly influences the fit results, it was not included in the comparison.

EXAFS data with k = 3 – 10 Å^{-1} was Fourier transformed and fitted between R = 1.1 – 2.9 Å to the first and second neighbors of Ti in TiC_{calc}. Data from the 1300 K sample was used to derive the energy origin shift, ΔE, which was hold as a fixed parameter during all fits (ΔE_C = 3.41 eV, ΔE_{Ti} = 0.86 eV). Fig. 7 shows the back-Fourier transformed data (R = 1.1 and 2.9 Å) for all a-C:Ti specimen as solid lines. The fits are represented as dashed lines. Tab. 1 summarizes results of the fittings.

Data of the 1300 K and 1100 K annealed specimen are well described by the TiC_{calc} model. Ti-C distance for both temperatures is similar, but Ti-Ti distance is significantly lower for 1100 K. The derived Debye-Waller factor σ^2 is a measure of the statistical disorder of the scatterer positions. It decreases for both shells from 1100 K to 1300 K which shows an increase of order in the first two shells.

For the 700 K annealed specimen, significant differences between data and fit for the higher k region is observed (Fig. 7). Higher σ^2 values correspond to more disorder in the first two shells. The Ti-Ti distance further decreased, but the Ti-C distance R_{Ti-C} is larger than for the higher annealed samples. This could be due to the fact that the first shell is a combination of two different bonding states: One fraction of Ti atoms has carbon in TiC-like arrangement in the first shell; the other Ti atoms are surrounded by an amorphous carbon matrix with higher Ti-C distance than for TiC. This is in correspondence with the values for the second shell: Ti as second neighbor is visible but with lower intensity as indicated by the smaller amp_{Ti-Ti} value. This shows that no significant number of TiC-like crystals is present.

The derived values for the as-deposited layer show a further increased amorphous coordination in the first two shells of Ti as compared to the 700 K annealed layer.

Obviously, TiC_{calc} does not satisfactorily represent the structural environment of Ti in the as deposited layers.

The decrease of amp_{Ti-Ti} with lower annealing temperature reflects the decreasing size of TiC-like agglomerates in the a-C matrix, which results in less Ti-Ti pairs at the distance characteristic for a TiC-like structure. Annealing to 700 K seems mainly to increase the order in the first two shells, but does not lead to a significant formation of TiC-like crystallites. For the as-deposited layer almost no TiC like agglomerates should be present.

The increase of R_{Ti-Ti} from the as-deposited to the 1300 K annealed layer could be explained in that way, that for lower annealing temperatures the small TiC-like crystallites are not perfectly stoichiometric, which results in decreased average Ti-Ti distance due to missing carbon atoms in the first shell.

4. Summary

Combining the fitting results with the qualitative comparison of EXAFS spectra, the low intensity of EXAFS oscillations in the as-deposited sample is consistent with a highly amorphous environment of Ti. Also, only a low number of Ti atoms appear in the neighboring shells of Ti, which is much stronger electron backscatterer than carbon. This indicates that there should be virtually no TiC-like aggregates; most Ti atoms should be homogenously distributed in an amorphous carbon matrix. Annealing to 700 K results in a slightly more ordered, but still mainly amorphous structure and a small increase of Ti atoms with TiC-like bonding environment in the first two shells. After annealing to 1100 K the situation changes drastically. The Ti bonding environment is similar to that in TiC, Ti is well present in the second shell shells which shows that

diffusion of Ti occurred to form larger TiC crystallites. Annealing to 1300 K further increases the order of the first and second shell and results in larger TiC grain sizes. This is reflected in the appearance of additional maxima at higher distances (Fig. 6) and visible signals in the XRD spectrum.

The presented EXAFS investigations provides valuable additional information for the structural situation in a-C:Ti layers, because XRD showed distinct TiC crystallites only after heating to 1300 K.

Acknowledgement

The authors thank Dr. E. Welter, HASYLAB and M. Fußeder, IPP for assistance during EXAFS measurements. This work was supported by the European Community - Research Infrastructure Action under the FP6 "Structuring the European Research Area" Programme through the Integrated Infrastructure Initiative "Integrating Activity on Synchrotron and Free Electron Laser Science".

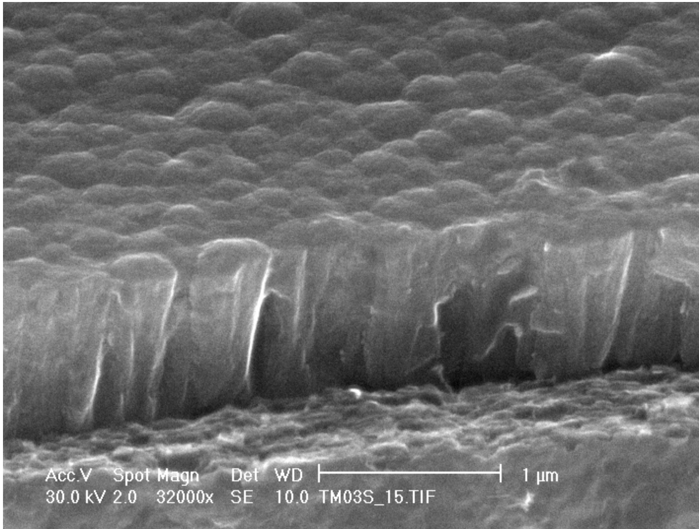

Fig. 1: SEM cross-section micrograph of an a-C:Ti sandwich layer (a-C/a-C:Ti/a-C) on graphite substrate.

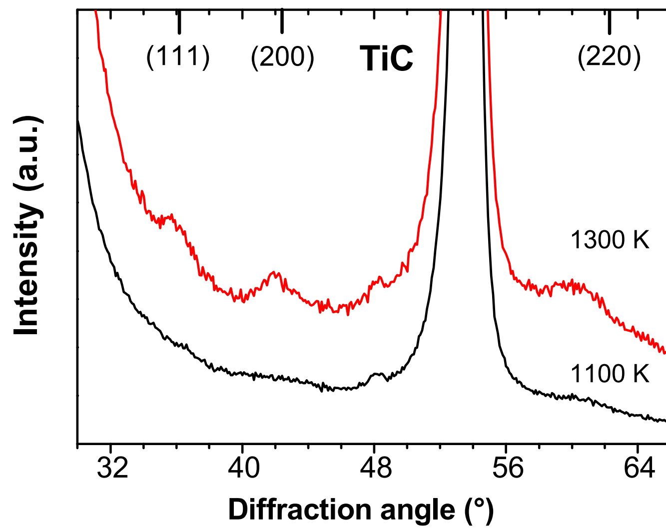

Fig 2: XRD spectra of a-C:Ti layers, heated at 1100 and 1300 K for 2 h. Peak positions for TiC are labeled.

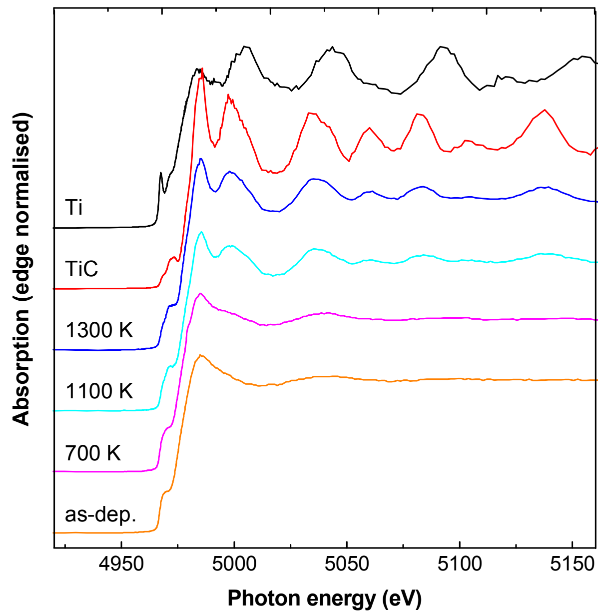

Fig 3: Ti *K*-edge XAS spectra of the a-C:Ti sandwich layers (as deposited, annealed for 2 h at 700, 1100 and 1300 K). Reference spectra of Ti and TiC (after correction for self-absorption) are shown for comparison. All spectra have been normalized to unit edge step.

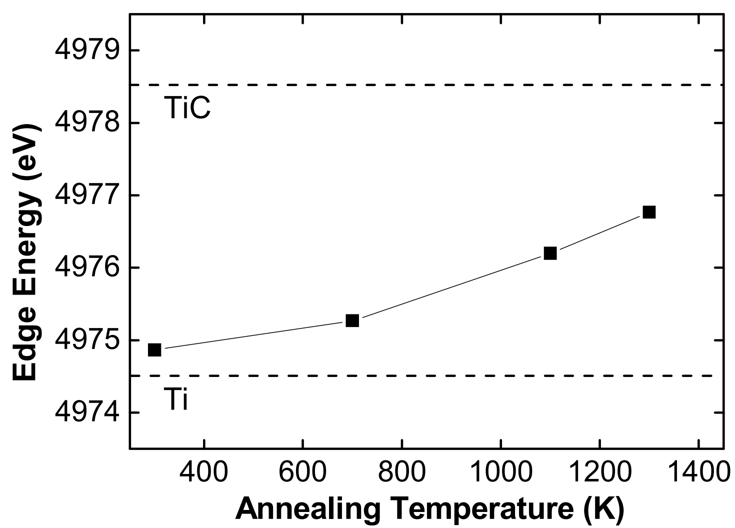

Fig. 4: Variation of Ti *K*-edge energy with annealing temperature for different a-C:Ti samples. The edge energy for the Ti and TiC standard sample is indicated by the dashed line. The values are derived by determining the edge position at the half intensity of the normalized edge step.

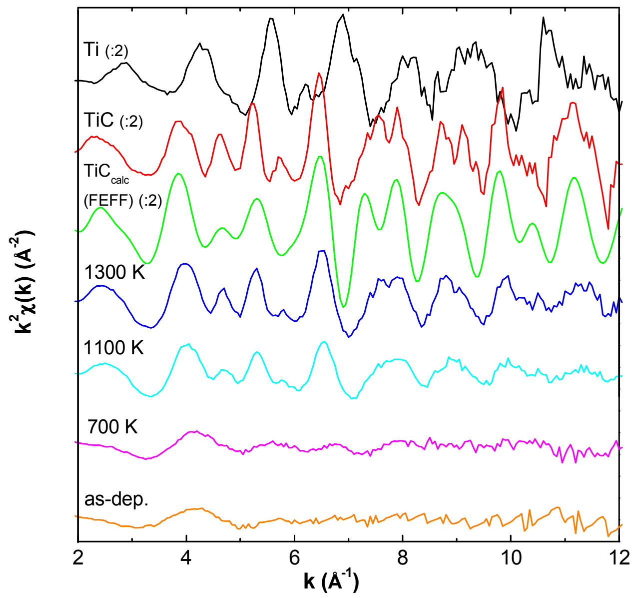

Fig. 5: k^2-weighted EXAFS, $k^2\chi(k)$, as a function of the photoelectron wave number k: a-C:Ti layers (as deposited, annealed at 700 K, 1100 K and 1300 K), Ti and TiC standard specimens, calculated TiC_{calc} using FEFF. Ti and TiC bulk standards and TiC_{calc} (cluster of 80 atoms) are plotted with half intensity.

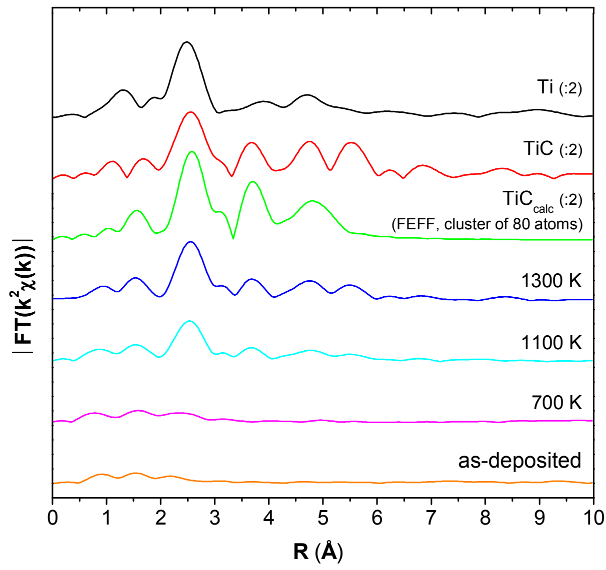

Fig 6: Magnitude of the non-phase-corrected Fourier transform of $k^2\chi(k)$ for a-C:Ti (as deposited, annealed to 700, 1100 and 1300 K). Phase correction would lead to a shift of ~ 0.4 Å [19]. Ti and TiC bulk standards and TiC_{calc} (cluster of 80 atoms) are plotted with half intensity.

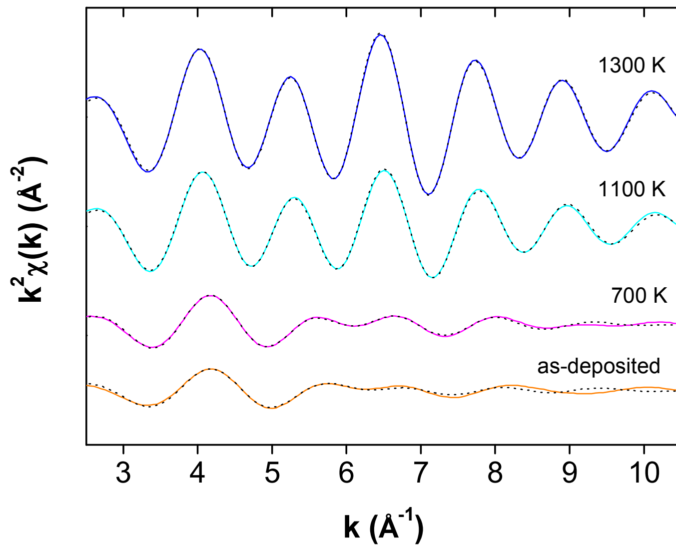

Fig. 7: Inverse Fourier transform of χ(R) in the region R = 1.1 – 2.9 Å for a-C:Ti specimen as deposited and annealed at 700 K, 1100 K and 1300 K. Solid lines represents experimental data, dashed lines show the result of a fit to the TiC_{calc} model for the first (Ti-C) and second shell (Ti-Ti).

Table 1: Fit results derived by fitting FEFF calculated TiC to EXAFS data for as deposited and annealed a-C:Ti specimen. Fitting of the first (Ti-C) and second (Ti-Ti) shell was performed in R-space between R = 1.1 and 2.9 Å.

a-C:Ti	R_{Ti-C}	σ^2_{Ti-C}	amp_{Ti-C}	R_{Ti-Ti}	σ^2_{Ti-Ti}	amp_{Ti-Ti}	R-factor
1300 K	2.141 ± 0.009	0.004 ± 0.003	0.55 ± 0.11	3.034 ± 0.003	0.002 ± 0.001	0.41 ± 0.04	0.002
1100 K	2.137 ± 0.007	0.007 ± 0.004	0.50 ± 0.12	3.019 ± 0.004	0.005 ± 0.001	0.36 ± 0.05	0.004
700 K	2.170 ± 0.021	0.012 ± 0.009	0.41 ± 0.22	2.948 ± 0.019	0.017 ± 0.010	0.20 ± 0.15	0.015
initial	2.202 ± 0.035	0.021 ± 0.018	0.60 ± 0.51	2.905 ± 0.046	0.013 ± 0.019	0.08 ± 0.11	0.068

[1] D. Nilsson, F. Svahn, U. Wiklund, S. Hogmark, Wear 254 (2003) 1084-1091.

[2] A. A. Voevodin, J. P. O'Neill, J. S. Zabinski, Thin Solid Films 342 (1999) 194-200.

[3] S. Yang, X. Li, N. M. Renevier, D. G. Teer, Surface & Coatings Technology 142 (2001) 85-93.

[4] Q. F. Huang, S. F. Yoon, Rusli, H. Yang, B. Gan, K. Chew, J. Ahn, Journal of Applied Physics 88 (2000) 4191-4195.

[5] T. You, O. Niwa, T. Horiuchi, M. Tomita, Y. Iwasaki, Y. Ueno, S. Hirono, Chemistry of Materials 14 (2002) 4796-4799.

[6] R. Aymar, Journal of Nuclear Materials 307 (2002) 1-9.

[7] M. Balden, C. Garcia-Rosales, R. Behrisch, J. Roth, P. Paz, J. Etxeberria, Journal Of Nuclear Materials 290 (2001) 52-56.

[8] E. d. J. Pardo, M. Balden, B. Cieciwa, C. Garcia-Rosales, J. Roth, Physica Scripta T111 (2004) 62-67.

[9] M. Balden, E. D. Pardo, I. Quintana, B. Cieciwa, J. Roth, Journal of Nuclear Materials 337-39 (2005) 980-984.

[10] M. Stuber, H. Leiste, S. Ulrich, H. Holleck, D. Schild, Surface & Coatings Technology 150 (2002) 218-226.

[11] B. Feng, D. M. Cao, W. J. Meng, J. Xu, R. C. Tittsworth, L. E. Rehn, P. M. Baldo, G. L. Doll, Surface & Coatings Technology 148 (2001) 153-162.

[12] W. J. Meng, R. C. Tittsworth, J. C. Jiang, B. Feng, D. M. Cao, K. Winkler, V. Palshin, Journal of Applied Physics 88 (2000) 2415-2422.

[13] M. Balden, B. T. Cieciwa, I. Quintana, E. de Juan Pardo, F. Koch, M. Sikora, B. Dubiel, Surface and Coatings Technology 200 (2005) 413-417.

[14] M. Mayer, SIMNRA User's Guide, Tech. Rep. IPP 9/113, Max-Planck-Institut für Plasmaphysik, Garching (1997).

[15] B. D. Cullity, Addison-Wesley (1967).

[16] B. Ravel, M. Newville, Journal of Synchrotron Radiation 12 (2005) 537-541.

[17] A. L. Ankudinov, B. Ravel, J. J. Rehr, S. D. Conradson, Physical Review B 58 (1998) 7565-7576.

[18] B. Ravel, Journal of Synchrotron Radiation 8 (2001) 314-316.

[19] D. C. Koningsberger, R. Prins, X-Ray Absorption. Principles, Applications, Techniques of EXAFS, SEXAFS and XANES, John Wiley & Sons, New York, 1988.